nature medicine

Tau deficiency induces parkinsonism with dementia by impairing APP-mediated iron export

Peng Lei[1,2], Scott Ayton[1,3], David I Finkelstein[1,3], Loredana Spoerri[2,4], Giuseppe D Ciccotosto[1,2,4], David K Wright[5], Bruce X W Wong[1], Paul A Adlard[1,2], Robert A Cherny[1], Linh Q Lam[1], Blaine R Roberts[1], Irene Volitakis[1], Gary F Egan[5,6], Catriona A McLean[2], Roberto Cappai[2,4], James A Duce[1,3] & Ashley I Bush[1,2]

The microtubule-associated protein tau has risk alleles for both Alzheimer's disease and Parkinson's disease and mutations that cause brain degenerative diseases termed tauopathies[1–4]. Aggregated tau forms neurofibrillary tangles in these pathologies[3,5], but little is certain about the function of tau or its mode of involvement in pathogenesis. Neuronal iron accumulation has been observed pathologically in the cortex in Alzheimer's disease[6,7], the substantia nigra (SN) in Parkinson's disease[8–11] and various brain regions in the tauopathies[11,12]. Here we report that tau-knockout mice develop age-dependent brain atrophy, iron accumulation and SN neuronal loss, with concomitant cognitive deficits and parkinsonism. These changes are prevented by oral treatment with a moderate iron chelator, clioquinol. Amyloid precursor protein (APP) ferroxidase activity couples with surface ferroportin to export iron, but its activity is inhibited in Alzheimer's disease, thereby causing neuronal iron accumulation[7]. In primary neuronal culture, we found loss of tau also causes iron retention, by decreasing surface trafficking of APP. Soluble tau levels fall in affected brain regions in Alzheimer's disease and tauopathies[13–15], and we found a similar decrease of soluble tau in the SN in both Parkinson's disease and the 1-methyl-4-phenyl-1,2,3,6-tetrahydropyridine (MPTP) mouse model. These data suggest that the loss of soluble tau could contribute to toxic neuronal iron accumulation in Alzheimer's disease, Parkinson's disease and tauopathies, and that it can be rescued pharmacologically.

As little is known about the status of tau in Parkinson's disease, we examined tau forms in postmortem samples from people affected with Parkinson's disease and controls. Soluble tau levels in the SN were significantly lower in people with Parkinson's disease compared to age-matched, non–Parkinson's disease controls (44% lower; $P < 0.001$; **Fig. 1a** and **Supplementary Tables 1** and **2**), which is similar to affected brain regions in Alzheimer's disease and tauopathies[13–15]. The tau loss was independent of neuronal loss, and L-DOPA treatment did not influence tau levels in mice (**Supplementary Fig. 1**). There were no changes in insoluble tau in the SN or soluble tau of neocortex and cerebellum in Parkinson's disease, despite a widespread increase in hyperphosphorylated tau and a lower ratio of three-repeat tau to four-repeat tau (**Supplementary Table 2**).

Elevated SN iron has been reported in cases of Parkinson's disease[8–11], although its role has been debated. Soluble tau loss and high iron levels were distributed in similar locations in the brain affecting SN (iron levels 39% higher than control cases; $P = 0.004$; **Fig. 1a**) but not neocortex or cerebellum (**Supplementary Table 2**). Additionally, soluble tau and iron levels in the SN correlated in healthy tissue ($R^2 = 0.3768$; $P = 0.0067$; **Fig. 1b**) but not in Parkinson's disease (**Supplementary Fig. 2**). In the MPTP mouse model, iron elevation may be pathogenic, as the Parkinson's phenotype is rescued by overexpression of ferritin or treatment with iron chelators[16,17]. We found a reciprocal association between changes of SN tau and iron over 45 d in MPTP-intoxicated mice (**Fig. 1c** and **Supplementary Fig. 3**). Nigral tau levels declined significantly from the baseline by day 3 after MPTP treatment (39% decline; $P = 0.012$) and remained suppressed through day 45. At the same time, SN iron increased, reaching levels significantly above untreated littermate controls from day 21 (21% higher; $P = 0.027$; **Fig. 1c**).

We hypothesized that the gradual loss of SN iron homeostasis after MPTP treatment might be caused by upstream tau loss and would cause SN neurodegeneration. To test this, we examined tau-knockout mice[18], which are reported to show only minor abnormalities up to 7 months of age[18–22]. As tau-related pathology is linked to advanced aging, we hypothesized that tau-knockout mice might develop a degenerative phenotype with greater age. Indeed, although at 6 months of age the knockout mice performed indistinguishably from wild-type (WT) mice, at 12 months tau-knockout mice showed a severe decline in locomotor functions, evidenced by significantly greater time to turn ($P < 0.001$ compared to 12-month-old WT mice; $P < 0.001$ compared to 6-month-old knockout mice) and to complete the pole test ($P = 0.002$ compared to 12-month-old WT; $P = 0.003$ compared to 6-month-old knockout), reduced latency to

[1]Mental Health Research Institute, The University of Melbourne, Victoria, Australia. [2]Department of Pathology, The University of Melbourne, Victoria, Australia. [3]Centre for Neuroscience, The University of Melbourne, Victoria, Australia. [4]Bio21 Molecular Science and Biotechnology Institute, The University of Melbourne, Victoria, Australia. [5]Florey Neuroscience Institutes, The University of Melbourne, Victoria, Australia. [6]Present address: Monash Biomedical Imaging, Monash University, Clayton, Victoria, Australia. Correspondence should be addressed to A.I.B. (ashleyib@unimelb.edu.au)

Received 25 August 2011; accepted 29 November 2011; published online 29 January 2012; doi:10.1038/nm.2613

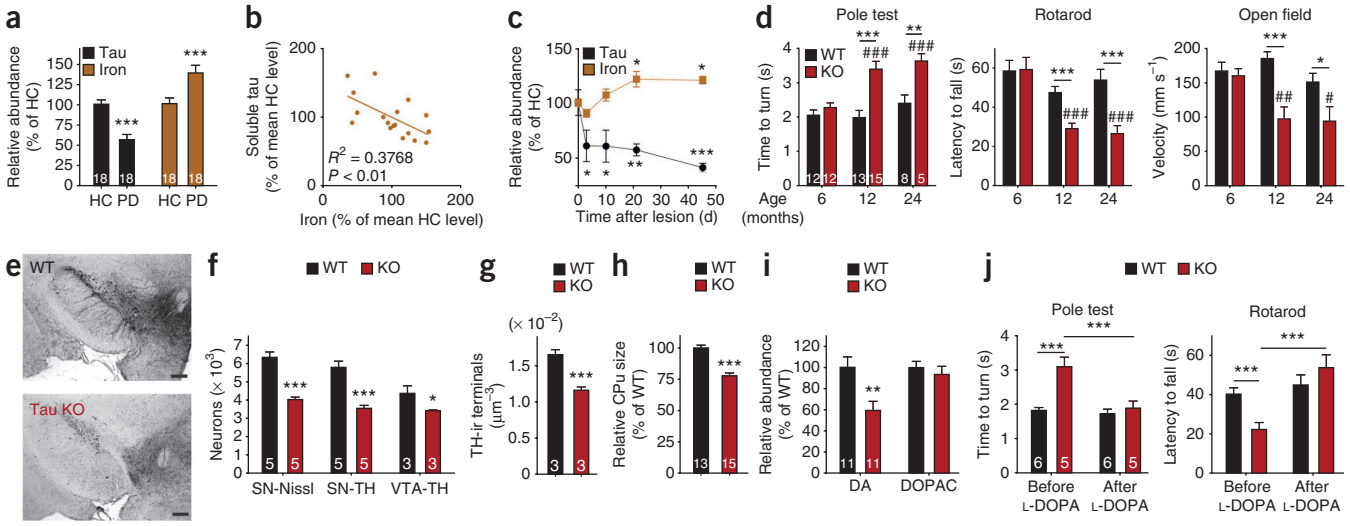

Figure 1 Tau loss is associated with the Parkinson's phenotype. (**a**) Levels of soluble tau (analyzed by blot densitometry) and iron in the SN of people with Parkinson's disease (PD) compared to age-matched healthy controls (HC), normalized to β-actin (tau) and protein (iron). (**b**) Correlation between soluble tau and iron in healthy controls. (**c**) SN tau and iron levels in mice treated with MPTP over time. $n = 10$ animals for each time point. Asterisks indicate significant changes from day 0 baseline. (**d**) Motor behavioral tests comparing performances between 6-, 12- and 24-month-old tau-knockout (KO) mice to age-matched background controls (WT). (**e**) Representative images of tyrosine hydroxylase (TH)-positive nigral neurons from WT and tau-KO mice. Scale bars, 250 μm. (**f**) Stereological count of Nissl-stained neurons in the SN and VTA. SN-Nissl, total number of neurons in the SN; SN-TH, total number of TH-immunoreactive neurons in the SN; VTA-TH, total number of TH-immunoreactive neurons in the VTA. (**g**) Stereological count (number of TH-immunoreactiver terminals per unit volume) of TH-ir terminals in the CPu. (**h**) CPu size. (**i**) Striatal dopamine (DA) and dihydroxyphenylacetic acid (DOPAC) levels. (**j**) Effects of L-DOPA treatment on performance in the pole test (left) and the rotarod test (right). Data in **e**–**i** are from 12-month-old mice. Error bars show means ± s.e.m., with n as indicated on bar graphs. $^{*}P < 0.05$, $^{**}P < 0.01$, $^{***}P < 0.005$ (versus age-matched WT); $^{\#}P < 0.05$, $^{\#\#}P < 0.01$, $^{\#\#\#}P < 0.005$ (versus 6-month-old tau KO).

fall in the rotarod test ($P < 0.001$ compared to 12-month-old WT; $P = 0.005$ compared to 6-month-old knockout), lower velocity ($P < 0.001$ compared to 12-month-old WT; $P = 0.002$ compared to 6-month-old knockout), shorter distance of locomotion ($P < 0.001$ compared to 12-month-old WT) and average distance of movement ($P < 0.001$ compared to 12-month-old WT; $P < 0.001$ compared to 6-month-old knockout) in the open field test, and shorter distance of movement in the Y maze ($P = 0.046$ compared to 12-month-old WT; $P = 0.05$ compared to 6-month-old knockout) (**Fig. 1d** and **Supplementary Fig. 4**). There were no further declines in these performance readouts in 24-month-old tau-knockout mice.

Motor deficits in Parkinson's disease are caused by nigral dopaminergic degeneration, dysregulated dopamine neurotransmission and decreased dopamine in the striatal projection field. L-DOPA, a precursor of dopamine[23], alleviates the motor symptoms. We found that there were 40% fewer dopaminergic (tyrosine hydroxylase–immunoreactive, TH-ir) neurons in the SN pars compacta in 12-month-old tau-knockout mice compared to age-matched WT mice ($P < 0.001$; **Fig. 1e**,**f**), consistent with the onset of motor loss. There were also significantly fewer TH-ir neurons in the ventral tegmental area (VTA; 22% fewer; $P = 0.016$; **Fig. 1f**), fewer TH-ir terminals in the caudate-putamen (CPu; 30% fewer; $P = 0.004$; **Fig. 1g**), smaller CPu size (22% smaller; $P < 0.001$; **Fig. 1h**) and lower striatal dopamine levels (42% lower; $P = 0.007$; **Fig. 1i**), as seen in Parkinson's disease itself[24,25]. These changes were not evident in 6-month-old animals (**Supplementary Fig. 5a**–**e**). A single dose of L-DOPA rescued motor deficits in 12-month-old tau-knockout mice, with complete recoveries of time to turn in the pole test ($P = 0.001$) and latency to fall in the rotarod test ($P < 0.001$) (**Fig. 1j**). Therefore, tau loss triggers a Parkinson's phenotype. As the SN neuron loss we observed in symptomatic mice is less extensive than the characteristic loss in Parkinson's disease toxin models[26], neuronal loss might act in concert with dysregulated dopamine neurotransmission to induce motor deficits in tau-knockout mice.

Examining other brain regions, we found that the wet brain weight of tau-knockout mice was significantly less than that of WT mice at 12 months of age (8% less; $P < 0.001$; **Fig. 2a**), but not at 6 months of age, whereas body weight was not different at either age (**Supplementary Fig. 6a**,**b**). Magnetic resonance imaging (MRI) of aged tau-knockout mice (18 months old) revealed conspicuous brain atrophy compared to age-matched WT mice (**Fig. 2b**). Examining postmortem brain sections from 12-month-old tau-knockout mice compared with WT mice, we found neocortical shrinkage (17%; $P < 0.001$), lateral ventricular enlargement (71%; $P = 0.033$) and cerebellar cortical thinning (loss of 7% of the granular cell layer; $P = 0.039$), but no change in corpus callosum or fourth ventricular size (**Fig. 2c**,**d**), consistent with the MRI findings. These neuroanatomical areas were unchanged in 6-month-old tau-knockout mice compared to WT mice (**Supplementary Fig. 6c**). Twelve-month-old tau-knockout mice were cognitively impaired in the Y maze task ($P = 0.041$ for duration; $P = 0.026$ for frequency; **Fig. 2e**), whereas 6-month-old tau-knockout mice performed indistinguishably from WT mice (**Supplementary Fig. 6d**,**e**). Compared with age-matched WT mice, tau-knockout mice at 12 months of age had smaller amounts of the neurotrophic support proteins BDNF (23% lower; $P = 0.01$), pro-BDNF (38% lower; $P = 0.004$) and TrkB (32% lower; $P = 0.044$) in the hippocampus (**Fig. 2f**), indicating that cognitive loss occurred in tandem with defects in neurotrophic support.

Consistent with the timing of behavioral and pathological changes, iron levels were significantly higher in the cortex (20% higher; $P = 0.005$), hippocampus (22%; $P = 0.039$) and SN (22%; $P = 0.04$) of 12-month-old tau-knockout mice compared to age-matched WT mice but

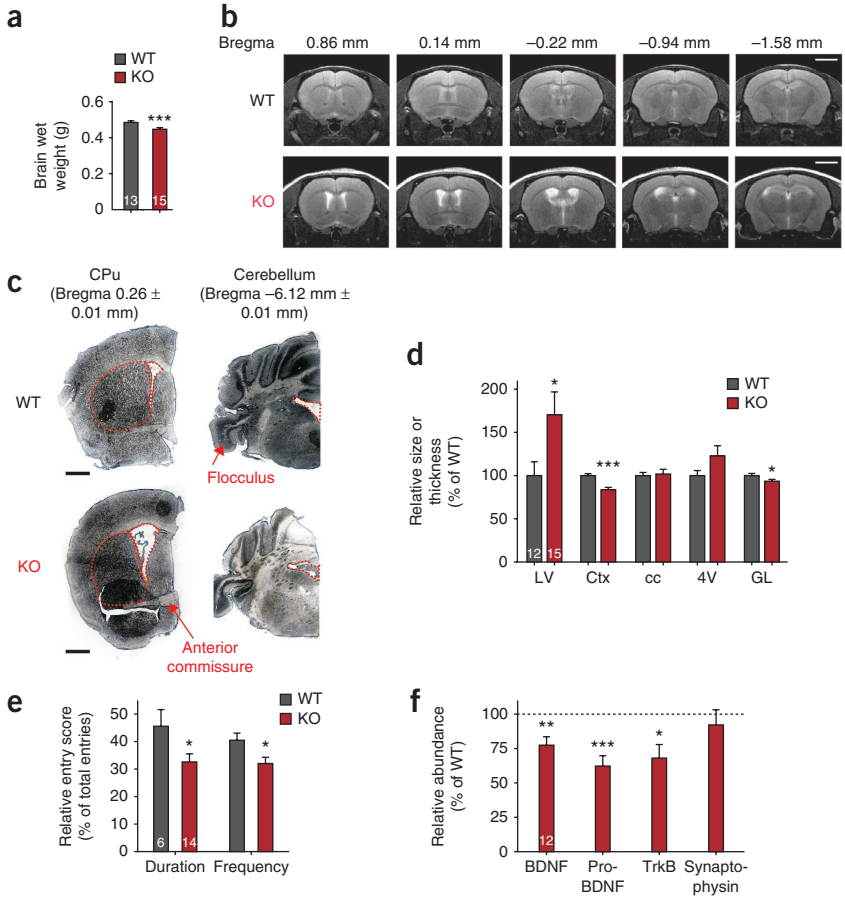

Figure 2 Age-dependent cognitive dysfunction in tau-KO mice. (**a**) Brain (including cerebellum) weights of 12-month-old tau-KO compared to WT mice. (**b**) Representative coronal MRI scans from 18-month-old WT and tau-KO mice. Scale bars, 2.5 mm. (**c**) Representative coronal sections of cerebrum (red dotted lines mark the CPu and lateral ventricle regions of interest) and cerebellum (red dotted lines mark the fourth ventricle). Scale bars, 1.25 mm. (**d**) Measurement of lateral ventricular area (LV), neocortical thickness (Ctx), corpus callosum thickness (cc), fourth ventricular area (4V) or granular layer thickness (GL). (**e**) Y-maze test for spatial learning and memory. (**f**) Analysis of hippocampal proteins in tau-KO mice by blot densitometry, normalized to β-actin. Data in **c**–**f** are from 12-month-old mice. Error bars show means ± s.e.m., with *n* as indicated on bar graphs. $^{*}P < 0.05$, $^{**}P < 0.01$, $^{***}P < 0.005$.

were unchanged in cerebellum or liver (**Fig. 3a**). Iron changes were not observed at 6 months of age in tau-knockout compared to WT mice (**Supplementary Fig. 7**). We examined the hippocampus and SN of 15-month-old tau-knockout and WT mice with Perls' and Turnbull's histology[7] and found that iron elevation in tau-knockout mice originated mostly from surviving neurons (**Fig. 3b**), as has been reported in Alzheimer's disease[6] and Parkinson's disease[10]. Both neuronal Fe(II) and Fe(III) were more abundant in tau-knockout mice (hippocampus, $P = 0.005$ and $P < 0.001$, respectively; SN, $P = 0.048$ and 0.046, respectively; **Fig. 3c**,**d**).

We tested whether the tau-knockout phenotype can be prevented by clioquinol, a moderate iron chelator that lowers SN iron abundance and rescues MPTP-induced Parkinsonism in mice[17]. Clioquinol (0.25 g per kg body weight, in food) was administered to tau-knockout mice from 6.5 months of age for 5 months. This treatment completely prevented the onset of neurodegeneration that developed in sham-treated mice during this period. Clioquinol treatment also prevented iron accumulation in hippocampus (11% less iron than untreated tau-knockout mice; $P = 0.025$) and SN (25% less iron; $P = 0.029$) (**Fig. 3e**). Liver iron levels were unaffected by clioquinol treatment (**Fig. 3e**), and neither copper nor zinc levels were altered by clioquinol in these tissues (**Supplementary Fig. 8**). Whereas tau-knockout mice on a normal diet developed motor deficits with aging, evidenced by the pole test ($P < 0.001$) (**Fig. 3f**) and rotarod test ($P = 0.043$) (**Supplementary Fig. 9a**), those whose diet contained clioquinol

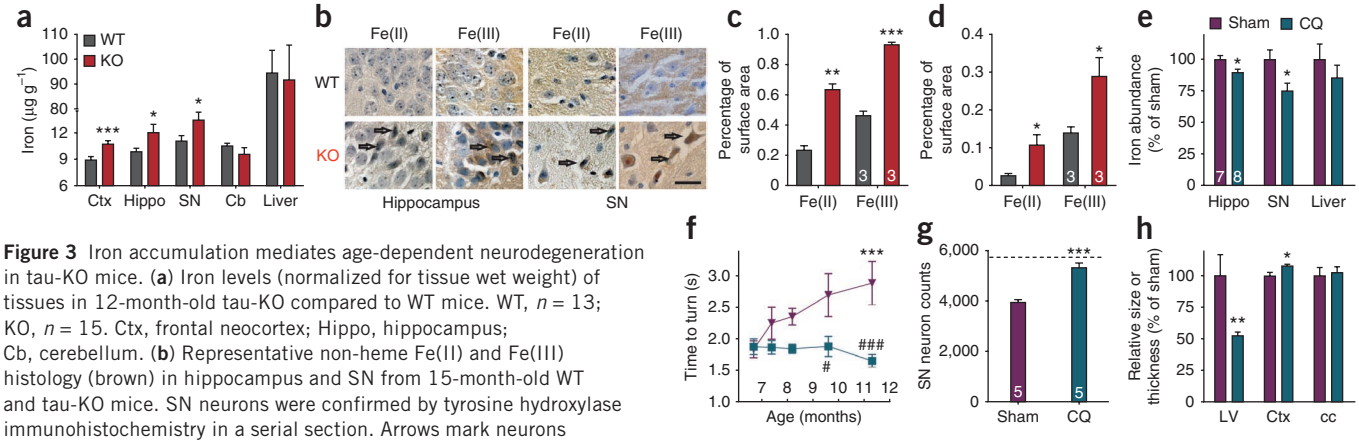

Figure 3 Iron accumulation mediates age-dependent neurodegeneration in tau-KO mice. (**a**) Iron levels (normalized for tissue wet weight) of tissues in 12-month-old tau-KO compared to WT mice. WT, $n = 13$; KO, $n = 15$. Ctx, frontal neocortex; Hippo, hippocampus; Cb, cerebellum. (**b**) Representative non-heme Fe(II) and Fe(III) histology (brown) in hippocampus and SN from 15-month-old WT and tau-KO mice. SN neurons were confirmed by tyrosine hydroxylase immunohistochemistry in a serial section. Arrows mark neurons affected by iron accumulation. Scale bar, 25 μm. (**c**,**d**) Computer-assisted quantification of Fe(II) and Fe(III) staining in hippocampus (**c**) and SN (**d**). (**e**–**h**) Effects of oral clioquinol (CQ) treatment of tau-KO mice (compared with sham treatment) on iron levels in hippocampus, SN and liver (**e**), age-dependent motor decline in the pole test (**f**), SN neuronal loss (**g**) and cortical atrophy (**h**). CQ treatment commenced at 6.5 months of age for 5 months. Dashed line in **g** represents the mean SN neuron count of 12-month-old WT mice. Error bars show means ± s.e.m. Sham, $n = 7$; CQ, $n = 8$ (in panels **f** and **h**), or as indicated on bar graphs. $^{*}P < 0.05$, $^{**}P < 0.01$, $^{***}P < 0.005$ (versus age 6.5 months in **f**); $^{\#}P < 0.05$, $^{\#\#\#}P < 0.005$ (versus sham treatment in **f**).

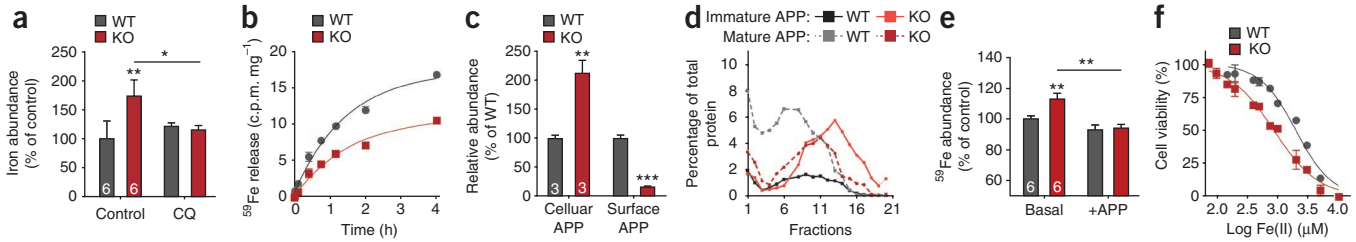

Figure 4 Knockout of tau causes iron accumulation by preventing APP trafficking to the cell surface. (**a**) Iron levels in primary cortical neurons (PCNs) from WT and tau-KO mice, and effects of CQ treatment (10 μM for 24 h). (**b**) ^{59}Fe efflux from PCNs of tau-KO compared to WT mice. Cultures were pretreated with ^{59}Fe-loaded transferrin. (**c**) Densitometric quantification of cellular (total) APP and surface (biotinylated) APP in PCNs of tau-KO compared to WT mice. (**d**) Distribution of immature and mature forms of APP in an iodixanol step gradient of PCNs from tau-KO compared to WT mice. Data are typical of three independent experiments. (**e**) ^{59}Fe retention in tau-KO and WT PCNs after incubation with ^{59}Fe-loaded transferrin, with or without soluble APP695α (APP; 1 μM). Data are normalized to abundance of ^{59}Fe in WT neurons without sAPP695α (Basal). (**f**) Survival curves of PCNs from tau-KO compared to WT mice, incubated with indicated $Fe(NH_4)_2(SO_4)_2$ concentrations for 48 h. Error bars show means ± s.e.m., with $n = 6$ (panels **b** and **f**) or as indicated on bar graphs. $^*P < 0.05$, $^{**}P < 0.01$, $^{***}P < 0.005$.

showed no sign of decline, performing significantly better than knockout mice on a normal diet in both tests ($P < 0.001$ and $P < 0.008$, respectively). Clioquinol treatment also prevented cognitive decline, as evidenced by improved novel arm frequency in the Y maze compared to the sham-treated group ($P = 0.028$; **Supplementary Fig. 9b**). Clioquinol treatment of the tau-knockout mice concomitantly prevented SN neuronal loss ($P < 0.001$; **Fig. 3g**) and CPu shrinkage (18% larger CPu; $P = 0.002$) (**Supplementary Fig. 9c**), and it resulted in higher striatal dopamine levels (**Supplementary Fig. 9d**). Clioquinol treatment also rescued lateral ventricular enlargement (53% smaller upon treatment; $P = 0.008$) and cortical thinning (8% thicker upon treatment; $P = 0.013$) that were observed in the tau-knockout mice (**Fig. 3h**). Therefore, tau deficiency causes iron accumulation in the brain and triggers neurodegeneration that is rescued by suppression of brain iron elevation with clioquinol.

We studied the mechanism of neuronal iron accumulation caused by lack of tau in primary cortical neurons from embryonic day 14, comparing WT and tau-knockout mice. Tau-knockout neurons retained significantly more iron (73% more; $P = 0.007$; **Fig. 4a**), but not copper or zinc (**Supplementary Fig. 10a**,**b**), after 7 d in culture. Treatment (24 h) with clioquinol normalized iron levels (**Fig. 4a**) without affecting copper or zinc (**Supplementary Fig. 9e**,**f**), consistent with the results in clioquinol-treated mice. Moreover, after incubation for 24 h with transferrin loaded with radioactive iron (^{59}Fe), tau-knockout neurons accumulated more ^{59}Fe than WT controls (19% more; $P = 0.042$), but this effect was not apparent after 1 h incubation (**Supplementary Fig. 10c**). Indeed, the iron efflux rate was significantly lower in tau-knockout neurons ($P < 0.001$; $n = 6$; **Fig. 4b**).

As tau modulates protein trafficking by stabilizing neuronal microtubules[3,5], we hypothesized that loss of tau impaired the trafficking of an iron efflux protein. The primary pathway for neuronal iron export is through the interaction of ferroportin (Fpn) with APP (full-length transmembrane and soluble forms), the sole export ferroxidase in neurons[7]. Tau has previously been shown to bind the C terminus of APP[27], and tau overexpression alters neuronal APP trafficking[28]. We found higher total APP levels in tau-knockout primary neurons compared to WT primary neurons (105% higher; $P = 0.008$; **Fig. 4c**), possibly caused by the higher iron levels inducing APP translation[29]. However, this increased APP did not function in iron export, as the amount detected by biotinylation at the neuronal surface was markedly lower in tau-knockout neurons compared to WT neurons (85% lower; $P < 0.001$; **Fig. 4c** and **Supplementary Fig. 10d**). Fpn levels were unaltered by tau loss (**Supplementary Fig. 10d**,**e**); therefore, tau deficiency causes iron accumulation by preventing the trafficking of APP to the neuronal surface where it must localize to act on Fpn[7].

We separated organelles from primary neurons through an iodixanol step gradient to determine the subcellular localization of APP (**Supplementary Fig. 10f**). Western blotting showed that in WT neurons APP had a broad distribution among fractions 5–12 and largely colocalized with tau; however, APP in tau-knockout neurons shifted to fractions 9–16 (**Supplementary Fig. 10g**). The endoplasmic reticulum (labeled with Bip) segregated to the bottom of the gradient (fractions 12–20), cosedimenting with immature forms of APP in tau-knockout neurons (**Fig. 4d**), indicating that loss of tau prevents APP from maturation and being trafficked toward the cell surface. This was also consistent with the lack of mature APP in intact tau-knockout neurons (**Supplementary Fig. 10d**). Adding soluble APP695α (1 μM) to the culture suppressed iron accumulation in tau-knockout neurons (**Fig. 4e**), suggesting that this treatment replaced the APP that did not traffic to the surface.

As iron export through the APP pathway prevents overload toxicity and oxidative stress[7], we tested the viability of primary neurons lacking tau compared to normal neurons under metal-stressed conditions. The half-maximal lethal dose (LD_{50}) for Fe(II) toxicity was 57% lower for tau-knockout neurons (869 μM) than for WT neurons (1,982 μM; $P < 0.001$; **Fig. 4f**), but LD_{50} values were unchanged for either Zn^{2+} or Cu^{2+} toxicity (**Supplementary Fig. 11a**,**b**), supporting the idea that tau is involved specifically in maintaining iron homeostasis.

Our data indicate that tau loss leads to neurotoxic iron accumulation. Tau-knockout mice may be a useful model of human neurodegenerative diseases as they recapitulated the age-dependent phenotype of both cognitive loss and parkinsonism. A caveat to this model is that degeneration does not progress after 12 months of age. We hypothesize that this may reflect compensatory mechanisms preventing further deterioration that, in humans, might be surmounted by the toxicity of hyperphosphorylated tau. The findings recast the role of tau in Alzheimer's disease, Parkinson's disease and tauopathies: rather than being merely a source of toxic intracellular aggregates, tau is also needed to prevent age-related damage. This is consistent with a published hypothesis that tau aggregates in disease may withdraw functional tau from the cytoplasm[13]. Further studies will determine whether hyperphosphorylation of tau, and pathogenic tau mutations (known to cause dementia[30] and parkinsonism[31,32] in transgenic mice), themselves induce a loss of iron-export function via effects on APP trafficking. Our findings prompt the hypothesis that the tau risk alleles for both Alzheimer's disease and Parkinson's

disease prime neurons for age-dependent deterioration by decreasing the efficiency of neuronal iron export. Therefore, strategies that maintain tau solubility and abundance may form the basis for new disease-modifying therapies.

METHODS

Methods and any associated references are available in the online version of the paper at http://www.nature.com/naturemedicine/.

Note: Supplementary information is available on the Nature Medicine website.

ACKNOWLEDGMENTS

This work was supported by funds from the Australian Research Council, the National Health & Medical Research Council of Australia (NHMRC) and the Alzheimer's Association. The Victorian Brain Bank Network is supported by The University of Melbourne, The Mental Health Research Institute, The Alfred Hospital and the Victorian Forensic Institute of Medicine, and funded by Neurosciences Australia and the NHMRC. The authors thank Y.-H. Hung, H. Kim, S.H. Bush and A. Sedjahtera for helpful discussion and technical assistance, H.N. Dawson (Duke University) for providing the tau-knockout mice, and T.A. Rouault and D.L. Zhang (US National Institutes of Health) for MAP23 antibody.

AUTHOR CONTRIBUTIONS

P.L. and A.I.B. conceived of the study. A.I.B. raised funds for the study. P.L., S.A., J.A.D., L.S., D.K.W., P.A.A., D.I.F. and A.I.B. designed and performed the experiments. G.D.C., B.X.W.W., L.Q.L., B.R.R., I.V. and C.A.M. assisted with the experiments. G.F.E., P.A.A., R.A.C., R.C., D.I.F. and A.I.B supervised the experiments. P.L. and A.I.B. analyzed the data and wrote drafts of the manuscript. All authors edited the manuscript.

COMPETING FINANCIAL INTERESTS

The authors declare competing financial interests: details accompany the full-text HTML version of the paper at http://www.nature.com/naturemedicine/.

Published online at http://www.nature.com/naturemedicine/.
Reprints and permissions information is available online at http://www.nature.com/reprints/index.html.

1. Laws, S.M. *et al.* Fine mapping of the MAPT locus using quantitative trait analysis identifies possible causal variants in Alzheimer's disease. *Mol. Psychiatry* **12**, 510–517 (2007).
2. Laws, S.M. *et al.* Genetic analysis of MAPT haplotype diversity in frontotemporal dementia. *Neurobiol. Aging* **29**, 1276–1278 (2008).
3. Lei, P. *et al.* Tau protein: relevance to Parkinson's disease. *Int. J. Biochem. Cell Biol.* **42**, 1775–1778 (2010).
4. Höglinger, G.U. *et al.* Identification of common variants influencing risk of the tauopathy progressive supranuclear palsy. *Nat. Genet.* **43**, 699–705 (2011).
5. Lee, V.M.-Y., Goedert, M. & Trojanowski, J.Q. Neurodegenerative tauopathies. *Annu. Rev. Neurosci.* **24**, 1121–1159 (2001).
6. Smith, M.A., Harris, P.L., Sayre, L.M. & Perry, G. Iron accumulation in Alzheimer disease is a source of redox-generated free radicals. *Proc. Natl. Acad. Sci. USA* **94**, 9866–9868 (1997).
7. Duce, J.A. *et al.* Iron-export ferroxidase activity of β-amyloid precursor protein is inhibited by zinc in Alzheimer's disease. *Cell* **142**, 857–867 (2010).
8. Bartzokis, G. *et al.* MRI evaluation of brain iron in earlier- and later-onset Parkinson's disease and normal subjects. *Magn. Reson. Imaging* **17**, 213–222 (1999).
9. Zecca, L., Youdim, M.B., Riederer, P., Connor, J.R. & Crichton, R.R. Iron, brain ageing and neurodegenerative disorders. *Nat. Rev. Neurosci.* **5**, 863–873 (2004).
10. Oakley, A.E. *et al.* Individual dopaminergic neurons show raised iron levels in Parkinson disease. *Neurology* **68**, 1820–1825 (2007).
11. Dexter, D.T., Jenner, P., Schapira, A.H. & Marsden, C.D. Alterations in levels of iron, ferritin, and other trace metals in neurodegenerative diseases affecting the basal ganglia. The Royal Kings and Queens Parkinson's Disease Research Group. *Ann. Neurol.* **32** (suppl.), S94–S100 (1992).
12. Paisán-Ruiz, C. *et al.* Widespread Lewy body and tau accumulation in childhood and adult onset dystonia-parkinsonism cases with PLA2G6 mutations. *Neurobiol. Aging* (in the press).
13. Khatoon, S., Grundke-Iqbal, I. & Iqbal, K. Levels of normal and abnormally phosphorylated tau in different cellular and regional compartments of Alzheimer disease and control brains. *FEBS Lett.* **351**, 80–84 (1994).
14. Ksiezak-Reding, H., Binder, L.I. & Yen, S.-H.C. Immunochemical and biochemical characterization of tau proteins in normal and Alzheimer's disease brains with Alz 50 and Tau-1. *J. Biol. Chem.* **263**, 7948–7953 (1988).
15. Zhukareva, V. *et al.* Selective reduction of soluble tau proteins in sporadic and familial frontotemporal dementias: an international follow-up study. *Acta Neuropathol.* **105**, 469–476 (2003).
16. Mandel, S.A. *et al.* Multifunctional activities of green tea catechins in neuroprotection. Modulation of cell survival genes, iron-dependent oxidative stress and PKC signaling pathway. *Neurosignals* **14**, 46–60 (2005).
17. Kaur, D. *et al.* Genetic or pharmacological iron chelation prevents MPTP-induced neurotoxicity in vivo: a novel therapy for Parkinson's disease. *Neuron* **37**, 899–909 (2003).
18. Dawson, H.N. *et al.* Inhibition of neuronal maturation in primary hippocampal neurons from tau deficient mice. *J. Cell Sci.* **114**, 1179–1187 (2001).
19. Harada, A. *et al.* Altered microtubule organization in small-calibre axons of mice lacking tau protein. *Nature* **369**, 488–491 (1994).
20. Ikegami, S., Harada, A. & Hirokawa, N. Muscle weakness, hyperactivity, and impairment in fear conditioning in tau-deficient mice. *Neurosci. Lett.* **279**, 129–132 (2000).
21. Roberson, E.D. *et al.* Reducing endogenous tau ameliorates amyloid beta-induced deficits in an Alzheimer's disease mouse model. *Science* **316**, 750–754 (2007).
22. Ittner, L.M. *et al.* Dendritic function of tau mediates amyloid-beta toxicity in Alzheimer's disease mouse models. *Cell* **142**, 387–397 (2010).
23. Cookson, M.R. The biochemistry of Parkinson's disease. *Annu. Rev. Biochem.* **74**, 29–52 (2005).
24. O'Neill, J. *et al.* Quantitative 1H magnetic resonance spectroscopy and MRI of Parkinson's disease. *Mov. Disord.* **17**, 917–927 (2002).
25. Dauer, W. & Przedborski, S. Parkinson's disease: mechanisms and models. *Neuron* **39**, 889–909 (2003).
26. Sedelis, M., Schwarting, R.K. & Huston, J.P. Behavioral phenotyping of the MPTP mouse model of Parkinson's disease. *Behav. Brain Res.* **125**, 109–125 (2001).
27. Smith, M.A. *et al.* Tau protein directly interacts with the amyloid beta-protein precursor: implications for Alzheimer's disease. *Nat. Med.* **1**, 365–369 (1995).
28. Stamer, K., Vogel, R., Thies, E., Mandelkow, E. & Mandelkow, E.-M. Tau blocks traffic of organelles, neurofilaments and APP vesicles in neurons and enhances oxidative stress. *J. Cell Biol.* **156**, 1051–1063 (2002).
29. Rogers, J.T. *et al.* An iron-responsive element type II in the 5′-untranslated region of the Alzheimer's amyloid precursor protein transcript. *J. Biol. Chem.* **277**, 45518–45528 (2002).
30. Ramsden, M. *et al.* Age-dependent neurofibrillary tangle formation, neuron loss, and memory impairment in a mouse model of human tauopathy (P301L). *J. Neurosci.* **25**, 10637–10647 (2005).
31. Lewis, J. *et al.* Neurofibrillary tangles, amyotrophy and progressive motor disturbance in mice expressing mutant (P301L) tau protein. *Nat. Genet.* **25**, 402–405 (2000).
32. Ittner, L.M. *et al.* Parkinsonism and impaired axonal transport in a mouse model of frontotemporal dementia. *Proc. Natl. Acad. Sci. USA* **105**, 15997–16002 (2008).

ONLINE METHODS

Human postmortem brain tissues. We obtained postmortem tissues from the Victorian Brain Bank Network with informed consent from the individual or the individual's family. All procedures were approved by the Mental Health Research Institute Human Ethics Committee and were in accordance with the Australian National Health and Medical Research Council guidelines. Clinical information is described in **Supplementary Table 1**. SN from 18 subjects with clinically defined Parkinson's disease (11 male, 75.3 ± 1.5 years old) and 18 control individuals without, or with minimal, known neurological or psychiatric disorders (13 male, 77.3 ± 1.2 years old) were selected. In some studies there was sufficient substantia nigra tissue for comparisons of only $n = 10$ in each group (in healthy controls, six male, 77.9 ± 2.3 years old; in subjects with Parkinson's disease, seven male, 75.4 ± 1.9 years old). Other brain tissues (frontal cortex and cerebellum) were taken from a subset of the complete sample group and consisted of ten subjects with clinically defined Parkinson's disease (six male, 75.8 ± 2.1 years old) and ten control individuals (five male, 76.6 ± 2.1 years old). There were no significant differences in age or postmortem interval between these various cohorts. Soluble SN tau levels did not correlate with postmortem interval ($R^2 = 0.004$; $P = 0.796$). We stored tissues at −80 °C until use.

MPTP time-course study. We intoxicated five-month-old C57BL/6 male mice (Monash animal services) with four intraperitoneal injections of 10 mg per kg body weight MPTP (every 2 h in the same day) to give a final dose of 40 mg per kg body weight[33]. Mice were killed with an overdose of sodium pentobarbitone (Lethabarb; 100 mg per kg body weight) on days 3, 10, 21 and 45 after MPTP treatment, and we used untreated littermate controls (killed on day 10) for comparison.

Performance and treatment studies of tau-knockout mice. We used tau-knockout mice[18] and background C57BL/6/SV129 control mice for performance studies and for biochemical studies. L-DOPA, freshly dissolved in 0.9% (wt/vol) NaCl, 0.5% (wt/vol) sodium carboxymethylcellulose, 0.5% (vol/vol) benzyl alcohol and 0.4% (vol/vol) Tween-80, was administered orally with the use of an oroesophageal needle at 10 mg per kg body weight for one dose. We carried out the performance tests 1 h after the dose. For clioquinol treatment, tau-knockout mice commenced clioquinol feeding from 6.5 months of age. We fed mice a diet of rodent chow mixed with 0.25 g per kg body weight (equivalent to dosing of ~30 mg per kg body weight per day) of clioquinol (Specialty Feeds) for 5 months and then killed them for biochemical studies. We administered performance tests every 3–4 weeks to monitor the effects of clioquinol.

Recombinant APP expression and purification. We expressed soluble human APP695α in the methylotrophic yeast *Pichia pastoris* strain GS115 and purified as described[7]. Briefly, we performed a two-step procedure using an AKTA FPLC device (GE Healthcare). We purified APP695α from culture media using anion exchange on a Q-Sepharose column (1.6 cm × 25 cm column; GE Healthcare) followed by hydrophobic exchange with phenyl-Sepharose (0.5 cm × 5 cm column; GE Healthcare).

^{59}Fe-loaded transferrin preparation. We purified human apo-transferrin and then loaded it with ^{59}Fe (PerkinElmer) as described[7]. We incubated neurons with 1.0×10^{-6} M ^{59}Fe-loaded transferrin for various periods in serum-free Neurobasal-supplemented medium (Invitrogen). We then removed medium after 1 h or 24 h, and incubated neurons with or without soluble APP695α (1 μM), washed them thoroughly with PBS and harvested with trypsin. For the neuronal efflux assay, we incubated cells at 37 °C and removed medium at various time points. We performed a comparable time course at 4 °C to account for nonspecific binding of ^{59}Fe to the outer membrane. We measured all media and cell lysates by γ-ray counter (Wizard 3, PerkinElmer) in c.p.m.

Metal analysis. Samples from each experimental condition were freeze-dried and then resuspended in 69% nitric acid (ultraclean grade, Aristar) overnight. We then heated the samples for 20 min at 90 °C, and added an equivalent volume of hydrogen peroxide (30%; Merck) for a further 15 min incubation at 70 °C. We diluted the samples in double-distilled water and assayed them by an AA240 atomic absorption spectrometer (Varian) or inductively coupled plasma mass spectrometer (Ultramass 700, Varian). Each sample was measured in triplicate, and the concentrations determined from the standard curve were normalized to protein concentration or wet tissue weight.

Statistical analyses. Statistical analysis was carried out in Prism (GraphPad) or SPSS software. Before *t* tests or ANOVA *post hoc* tests were undertaken, a Leven's test for homogeneity of error variance was performed. For ANOVA, Dunnett's *post hoc t* tests were used when sample variances were homogeneous. Where variances between groups were found to differ significantly, Games-Howell *post hoc* tests were used. All tests were two-tailed, with the level of significance set at $P = 0.05$. Detailed tests used in each experiment are described in the **Supplementary Methods**.

Additional methods. Detailed methodology is described in the **Supplementary Methods**.

33. Przedborski, S. *et al.* The parkinsonian toxin 1-methyl-4-phenyl-1,2,3,6-tetrahydropyridine (MPTP): a technical review of its utility and safety. *J. Neurochem.* **76**, 1265–1274 (2001).

doi:10.1038/nm.2613